2011 IEEE/RSJ International Conference on
Intelligent Robots and Systems
September 25-30, 2011. San Francisco, CA, USA

Optimal energy density piezoelectric twisting actuators

Benjamin M. Finio and Robert J. Wood

Abstract— **The use of piezoelectric materials as actuators or sensors is widespread, and numerous actuator topologies and models have been developed. However, many of these applications do not place stringent requirements on actuator mass or energy density. Motivated by applications that do have strict requirements in these areas such as flapping-wing microrobots, a torsional piezoelectric actuator is developed. A model is presented that predicts output rotation, torque and energy density values; and allows optimization of these values based on actuator geometry. An emphasis is placed on actuator fabrication and testing for empirical validation of the model.**

I. Introduction

Piezoelectric actuators are commonly arranged as stacks or benders. Stacks provide small, high precision linear displacements while benders rely upon a cantilever configuration to transform curvatures into displacements (e.g. clamped-free cantilevers [1], [2], [3], "moonies" [4], and disks [5], [6]). Other than a means of applying an electrical field, stacks require no additional structures. Benders require an antagonist to generate a curvature; either an antagonistic piezoelectric layer (in the case of a bimorph) or a passive compliant layer. Twisting actuation has also been achieved through use of anisotropic composite materials or skewed orientation of piezoelectric plates [7], [8]. This paper describes the use of anisotropic passive layers laminated to a piezoelectric material to create a rotational actuator. The rotation is a function of in-plane anisotropy and anti-symmetric layering which combines to exploit extension-twisting coupling. Analytical models of such actuators have been presented previously for varying ply angles [9], here a model is presented which considers ply angles and geometries of the actuator as well as how induced strain from the piezoelectric layer couples into output torque.

The figures of merit of twisting angle and blocked torque are derived and the product is used tto produce rotary actuators with maximal energy density. However, the same modeling procedure can be used to design rotary actuators of any twist-torque value within the constraints allowed by the constituent materials and the converse piezoelectric effect. Using a meso-scale fabrication paradigm [10], we fabricate a variety of actuator geometries and measure twist and torque for model verification. Results prove the validity of the model as well as the value of this class of piezoelectric actuators. Such actuators could be used for a variety of applications from precision micro manipulation to high bandwidth power delivery.

Research was supported in part by the Army Research Laboratory (award number W911NF-08-2-0004) and by the Department of Defense (DoD) through the National Defense Science & Engineering Graduate Fellowship (NDSEG) Program.

The authors are with the School of Engineering and Applied Sciences and the Wyss Institute for Biologically Inspired Engineering, Harvard University, Cambridge, MA 02138. bfinio@fas.harvard.edu

II. Actuator Model

Twisting motion is achieved with a single piezoelectric layer by laminating antisymmetric top and bottom fiber-reinforced composite (FRC) layers (Fig. 1a). Thus an actuator of length L and width W can achieve a rotation angle of θ_{twist} (Fig. 1b) by applying a voltage across the piezoelectric layer (for d_{31} mode actuation), using the conductive FRC layers as electrodes (Fig. 1c). The following section presents derivation of the theory that predicts output twist angle, blocked torque and energy density based on the geometry and arrangements defined in Fig. 1.

A. Laminate Plate Theory

The model for a clamped-free piezoelectric cantilever actuator consisting of an arbitrary number of active piezoelectric and passive composite layers in arbitrary orientations is originally presented in [3], derived from the information in [11]. Here we use the same approach to derive the constitutive equations for unimorph twisting actuators.

First, assuming a state of plane stress for each layer (i.e. stresses act only in the $x-y$ plane since there are no surface tractions), the in-plane stresses are given by

$$\begin{bmatrix}\sigma_1\\ \sigma_2\\ \tau_{12}\end{bmatrix} = \begin{bmatrix}Q_{11} & Q_{12} & 0\\ Q_{12} & Q_{22} & 0\\ 0 & 0 & Q_{66}\end{bmatrix} \left(\begin{bmatrix}\epsilon_1\\ \epsilon_2\\ \gamma_{12}\end{bmatrix} - \begin{bmatrix}d_{31}\\ d_{32}\\ 0\end{bmatrix} E_3 \right) \quad (1)$$

where the subscripts 1, 2 and 3 correspond to a local coordinate system oriented with the fiber direction (Fig. 1a), E_3 is the electric field in the piezoelectric layer, and d_{31} and d_{32} are the electromechanical coupling coefficients of the piezoelectric material. Elements of the stiffness matrix $[Q]$ are defined as follows for an isotropic material (the piezoelectric layer in this case):

$$Q_{11} = Q_{22} = \frac{E}{1-\nu^2} \quad (2)$$

$$Q_{12} = \frac{E\nu}{1-\nu^2} \quad (3)$$

$$Q_{66} = \frac{E}{2(1+\nu)} = G \quad (4)$$

where E is the Young's modulus, G is the shear modulus and ν is the Poisson's ratio. For an anisotropic material (the

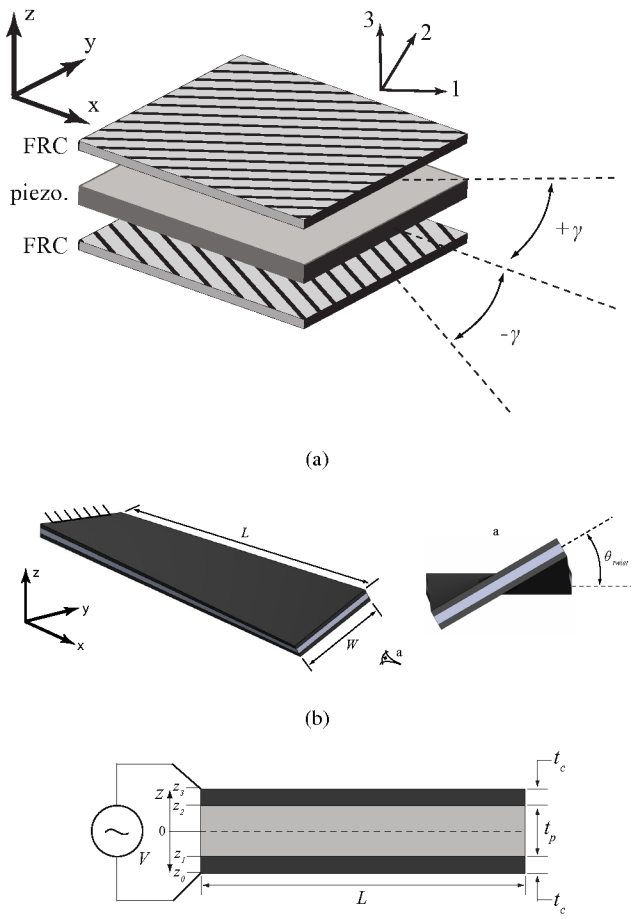

Fig. 1. (a) The fiber directions of the two fiber-reinforced composite (FRC) layers are oriented at angles of $\pm\gamma$ to the longitudinal axis of the actuator. This creates anisotropy in the compliance matrix and allows exploitation of extension-twisting coupling to create a twisting actuator. (b) A three-dimensional and end-on view of a twisting actuator with length L, width W, and twist angle θ_{twist}. (c) A cross-sectional view of an actuator, showing piezo layer thickness t_p, composite layer thickness t_c, the z-axis defined with $z = 0$ at the midplane, and electrical connections to the top and bottom composite layers.

FRC), elements of $[Q]$ are defined as

$$Q_{11} = \frac{E_1}{1 - \nu_{12}\nu_{21}} \tag{5}$$

$$Q_{12} = \frac{\nu_{12}E_2}{1 - \nu_{12}\nu_{21}} \tag{6}$$

$$Q_{22} = \frac{E_2}{1 - \nu_{12}\nu_{21}} \tag{7}$$

$$Q_{66} = G_{12} \tag{8}$$

where E_1 is the Young's modulus in the fiber direction, E_2 the modulus in the cross-fiber direction, and the following relationship holds:

$$\frac{\nu_{12}}{E_1} = \frac{\nu_{21}}{E_2} \tag{9}$$

To account for arbitrary orientation of anisotropic material layers, the stiffness matrix is modified:

$$\begin{bmatrix}\sigma_x\\ \sigma_y\\ \tau_{xy}\end{bmatrix} = \begin{bmatrix}\bar{Q}_{11} & \bar{Q}_{12} & \bar{Q}_{16}\\ \bar{Q}_{12} & \bar{Q}_{22} & \bar{Q}_{26}\\ \bar{Q}_{16} & \bar{Q}_{26} & \bar{Q}_{66}\end{bmatrix}\left(\begin{bmatrix}\epsilon_x\\ \epsilon_y\\ \gamma_{xy}\end{bmatrix} - \begin{bmatrix}d_{31}\\ d_{32}\\ 0\end{bmatrix}E_3\right) \tag{10}$$

where $[\bar{Q}_{ij}]$ is the adjusted stiffness matrix with the property

$$[\bar{Q}_{ij}] = [T]^{-1}[Q_{ij}][T]^{-T} \tag{11}$$

with the transformation matrix [T] defined as

$$[T] = \begin{bmatrix}m^2 & n^2 & 2mn\\ n^2 & m^2 & -2mn\\ -mn & mn & m^2 - n^2\end{bmatrix} \tag{12}$$

where $m = \cos(\gamma)$ and $n = \sin(\gamma)$ (Fig 1a).

To calculate overall deflections (displacements and/or rotations of the output), midplane strains and curvatures are integrated over the appropriate dimension. These strains and curvatures are given by

$$\begin{bmatrix}\epsilon^0\\ \kappa\end{bmatrix} = \begin{bmatrix}A & B\\ C & D\end{bmatrix}^{-1}\left(\begin{bmatrix}N^{ext}\\ M^{ext}\end{bmatrix} + \begin{bmatrix}N^p\\ M^p\end{bmatrix}\right) \tag{13}$$

where $\epsilon^0 = [\epsilon_x \quad \epsilon_y \quad \epsilon_{xy}]^T$, and $\kappa = [\kappa_x \quad \kappa_y \quad \kappa_{xy}]^T$. A, B and D are elements of the stiffness matrix defined as

$$A_{ij} = \sum_n [\bar{Q}_{ij}]_n (z_n - z_{n-1}) \tag{14}$$

$$B_{ij} = \frac{1}{2}\sum_n [\bar{Q}_{ij}]_n (z_n^2 - z_{n-1}^2) \tag{15}$$

$$C_{ij} = \frac{1}{3}\sum_n [\bar{Q}_{ij}]_n (z_n^3 - z_{n-1}^3) \tag{16}$$

where z_n is the height of the nth laminate layer with respect to the midplane of the structure (Fig. 1b).

N^{ext} and M^{ext} are the external forces and moments per unit width (i.e. $N = [N_x \quad N_y \quad N_{xy}]^T$, $M = [M_x \quad M_y \quad M_{xy}]^T$), and N^p and M^p are the piezoelectric forces and moments per unit width, defined as:

$$[N_i(E_3)]^p = \sum_n \int_{z_n-1}^{z_n} [\bar{Q}_{ij}]_n d_{3j} E_3 dz \tag{17}$$

$$[M_i(E_3)]^p = \sum_n \int_{z_n-1}^{z_n} [\bar{Q}_{ij}]_n d_{3j} E_3 z dz \tag{18}$$

Given Eq. 13, the maximum angle of twist, blocked torque, and energy density can be calculated for a given actuator geometry. The curvature element κ_{xy} is related to the vertical displacement of the actuator z as $\kappa_{xy} = \frac{\delta^2 z}{\delta x \delta y}$, therefore the angle of twist is calculated by evaluating the slope $\frac{\delta z}{\delta y}$ at the end of the beam:

$$\theta_{twist} = \tan^{-1}\left(\frac{\delta z}{\delta y}\Big|_{x=L}\right) \tag{19}$$

where L is the actuator length. Given the piezoelectric forces and moments from the converse piezoelectric effect (Eqs. 17 and 18) and assuming no external forces and moments, κ_{xy}

is calculated from Eq. 13, and $\frac{\delta z}{\delta y}$ at $x = L$ is calculated by integrating the curvature along the length of the beam:

$$\frac{\delta z}{\delta y}|_{x=L} = \int_0^L \kappa_{xy} dx \tag{20}$$

Since κ_{xy} is not a function of x, it is constant along the length of the beam. Combining Eqs. 19 and 20 yields a final expression for the angle of twist:

$$\theta_{twist} = \tan^{-1}(\kappa_{xy} L) \tag{21}$$

The blocked torque is defined as the external torque required to maintain zero twist angle when the piezoelectric material is activated. For convenience, the matrix C is defined as

$$C = \begin{bmatrix} A & B \\ B & D \end{bmatrix}^{-1} \tag{22}$$

From Eq. 13, assuming only an external M_{xy} is imposed and that piezoelectric moments are zero due to symmetry:

$$\kappa_{xy} = C_{66} M_{xy}^{ext} + C_{61} N_x^p + C_{62} N_y^p + C_{63} N_{xy}^p \tag{23}$$

This curvature can be broken down into two components: that due to the external moment and due to the piezoelectric forces. In order to maintain zero total twist, the superposition of these two curvatures must be zero, so Eq. 23 is used to solve for M_{xy}^{ext} by setting $\kappa_{xy} = 0$, and thus the blocked torque is:

$$\tau_b = -\frac{W}{C_{66}} \left(C_{61} N_x^p + C_{62} N_y^p + C_{63} N_{xy}^p \right) \tag{24}$$

where W is the actuator width (noting that M_{xy} is a moment per unit width).

Finally, given a maximum torque and maximum displacement, actuator energy density is calculated as the area under the torque-angle curve, normalized to actuator mass:

$$E_d = \frac{1}{2} \frac{\tau_b \theta_{max}}{m} \tag{25}$$

III. Experiments

A. Parameters

The model presented above can be used to design actuators with the best performance characteristics given certain metrics. For example micro grippers or manipulators may require a specific torque or rotation value, or a flying microrobot [12] may require optimal energy density given payload constraints. Several parameters of interest that can be varied experimentally are selected, namely

- Fiber layer orientation γ
- Actuator width W and length L
- Fiber layer thickness t_c

and the effects of varying these parameters on the following performance characteristics are examined:

- Output twist angle θ_{twist}
- Blocked torque τ_b
- Energy density E_d

These values can be calculated numerically with Eqs. 21, 24 and 25 respectively, and are compared to experimentally measured values. There are many additional experimental possibilities, such as application of an external load to determine actuator stiffness, frequency-domain analysis to determine resonant behavior, or use of a dynamometer to measure hysteresis effects, however those are beyond the scope of this work. A brief discussion of actuator fabrication and the experimental setup is presented here.

B. Fabrication

Actuators are fabricated using the techniques presented in [10]. Raw materials are cut with a custom-built laser micromachining system (355nm diode-pump solid state laser, Photonics Industries DC150H-355). Laser cut-files are made with a 2D CAD program (DWGEditor, Dassault Systems) and the laser system is operated with ProLase XP (American Laserware Inc.). Rectangular pieces of desired length, width, and angle in the case of the composite layer, are cut from bulk piezoelectric and carbon fiber composite sheets available in discrete thicknesses from the manufacturer (PZT-5H from Piezo Systems Inc. and M60J from Toray America respectively). Two carbon fiber layers and one piezoelectric layer are stacked to form the layup shown in Fig. 1 and vacuum bagged. The carbon fiber is pre-impregnated with a heat-curing epoxy, and the structure is cured under heat and pressure (with a Cascade TEK TFO-1 oven), bonding the layers together.

C. Experimental Setup

Actuator blocked torques (torque at zero rotation) were measured in a clamped-clamped configuration with a 6-axis Nano 17 force/torque sensor (ATI Industrial Automation). Data was recorded with data acquisition (DAQ) hardware and software supplied by ATI with the Nano17. Custom mechanical mounts were used to connect the actuators to mechanical ground and to interface with the sensor, and an XYZ micrometer stage and Labjack (Thorlabs Inc.) were used to allow precise alignment of the actuator's axis of rotation with the sensor's Z-axis. A custom Matlab script was used to generate actuator control signals which were conditioned through a high-voltage amplifier (Trek Inc.). The actuators were driven open-loop with no feedback. For information on feedback control of a voltage-driven piezoelectric actuator attached to a load, see [13].

Angle of twist was measured in a clamped-free configuration, using 2D motion tracking software (ProAnalyst, Xcitex Inc.) to calculate θ_{twist} from an edge-on view of the actuator (videos recorded with a PixeLink camera). A photograph and diagram of the experimental setup are shown in Fig. 2.

IV. Results

A. Fiber orientation

For fiber orientation tests, we expect a change in extension-twisting coupling due to changes in the compliance matrix (Eq. 22). These compliance changes give rise to varying torque/displacement to voltage relationships as predicted

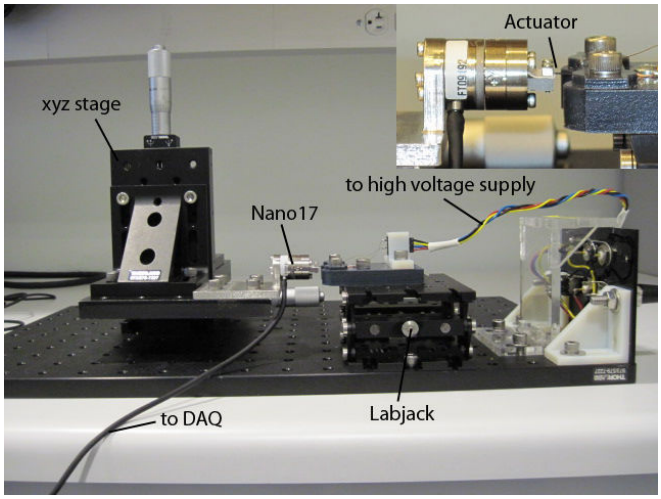

(a)

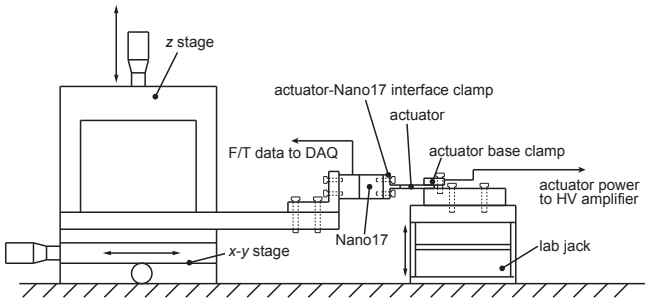

(b)

Fig. 2. (a) Photograph of experimental setup and (b) labeled diagram (not to scale).

in Sec. 2.1. For a fixed actuator width of $W = 2$mm, length of $L = 10$mm, and fiber layer thickness of $t_c = 80\mu$m, the orientation of the fiber layer was varied from 0 to 90 degrees. Test actuators were fabricated with 15 degree intervals in orientation (0, 15, 30, 45, 60, 75, 90), and the experimental results are compared to predictions in Fig. 3. The theoretical model predicts maximum performance at $\gamma = 45°$, with zero twist and torque at $\gamma = 0°$ and $\gamma = 90°$ (consistent with other models [9]). While the the model over-predicts rotation angle and under-predicts torque, the important figure of merit is that the experimental results follow the theoretical trend with maximum performance at $\gamma = 45°$.

B. Aspect ratio

Having determined that the optimal fiber orientation is $45°$, actuator length L and width W were varied for a fixed $\gamma = 45°$ and fiber thickness of 80μm. The model predicts that actuator rotation scales linearly with length but is independent of width, and vice versa for torque, leading to an energy density that is independent of both length and width (Figure 4). The constant energy density is roughly 1.0J/kg assuming an applied electric field of 1.57V/μm (200V applied across 127μm thick piezoelectric layer). Compare this to 0.15J/kg for a typical commercially available piezoelectric bending actuator [14] and 4.0J/kg as

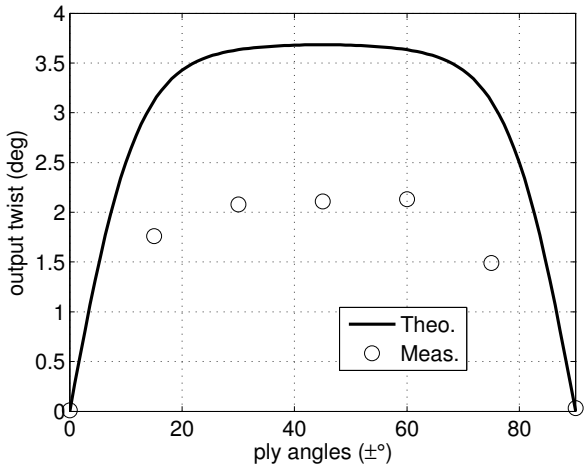

(a)

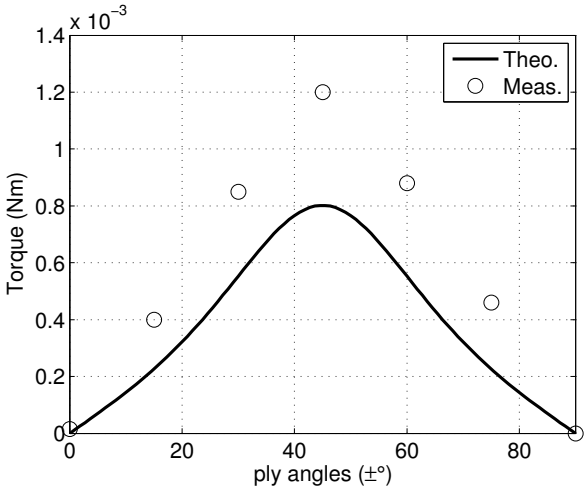

(b)

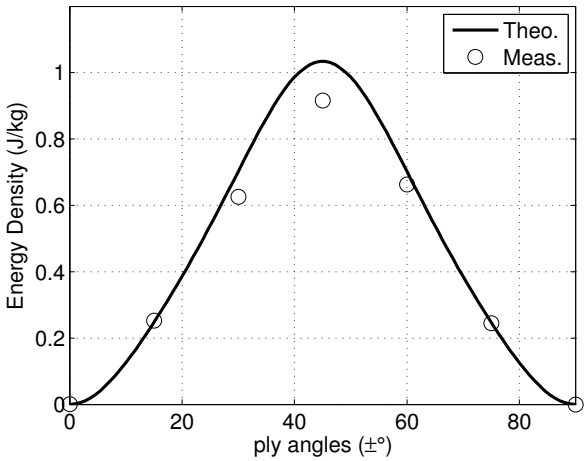

(c)

Fig. 3. (a) Theoretical and measured actuator rotation vs. fiber layer orientation, (b) blocked torque vs. fiber orientation, and (c) energy density vs. fiber orientation. The maximum performance occurs at $\gamma = 45°$.

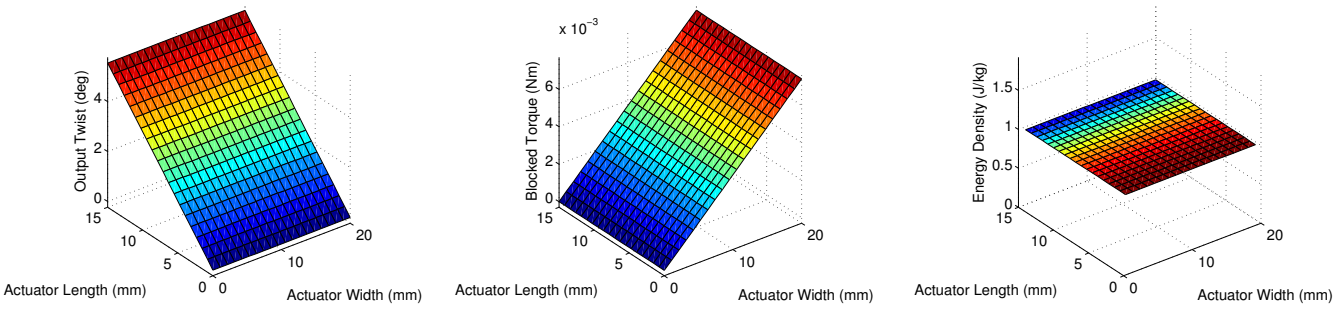

(a) (b) (c)

Fig. 4. (a) Actuator rotation vs. length and width, (b) blocked torque vs. length and width, and (c) energy density vs. length and width. All values are theoretical.

the maximum strain energy density for a bulk free plate of piezoelectric material [3]. Increasing the applied field to 2.36V/μm (300V across the same thickness) increases the predicted energy density to over 2.0J/kg, consistent with the results for bending actuators in [3]. Actuators of discrete lengths $L = 5$, 10 and 15mm and widths $W = 2$, 4 and 6mm were tested. The experimental results, presented in Figure 5, confirm that rotation depends only on length and torque depends only on width.

C. Fiber layer thickness

Finally, the effect of varying fiber layer thickness was investigated. Ability to manufacture actuators with variable thickness fiber layers is limited by the availability of materials from the manufacturer in discrete thicknesses (integer multiples of the thickness of a single sheet of material can be achieved by laminating multiple composite layers). As seen in Figure 6, there is a theoretical maximum rotation around $t_c = 25\mu$m, however carbon fiber sheets of this thickness were not available. Blocked torque increases indefinitely with increasing fiber thickness. Energy density depends on the product of these two terms, and Figure 6c shows that the rotation term dominates, i.e. the energy density has a global maximum and then decreases to zero. Fortunately this maximum occurs close to the range of commercially available thicknesses (50-80μm).

D. Optimal Performance

The analytical and empirical analyses determine fiber layer orientation γ and composite thickness t_c to be the most influential parameters when the primary performance criteria is energy density. Energy density is independent of actuator length and width, but since twist angle and torque scale linearly with these two values respectively, they can be adjusted as needed for the intended application.

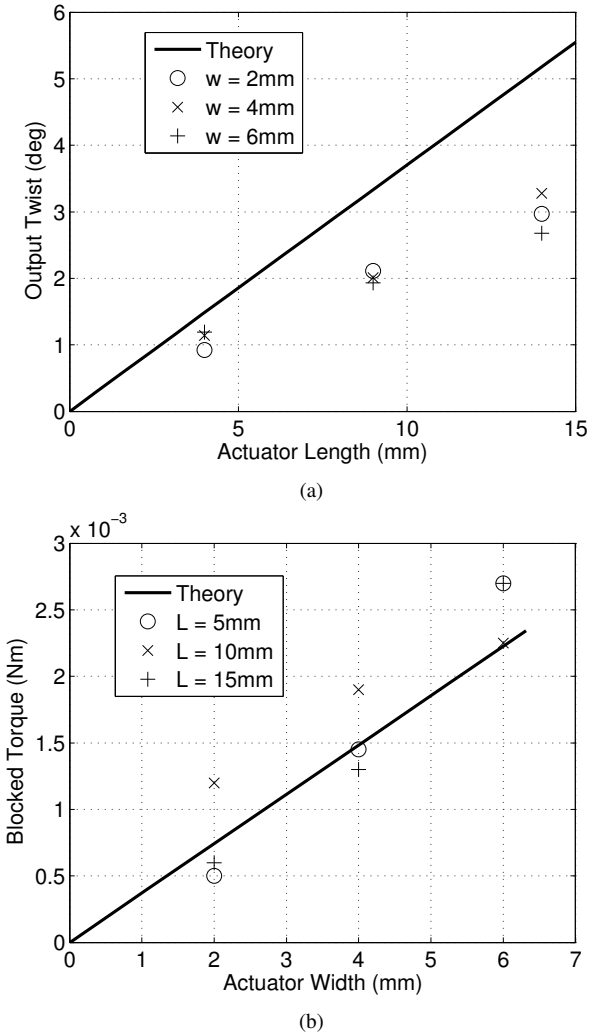

Fig. 5. (a) Actuator rotation vs. length and (b) blocked torque vs. width.

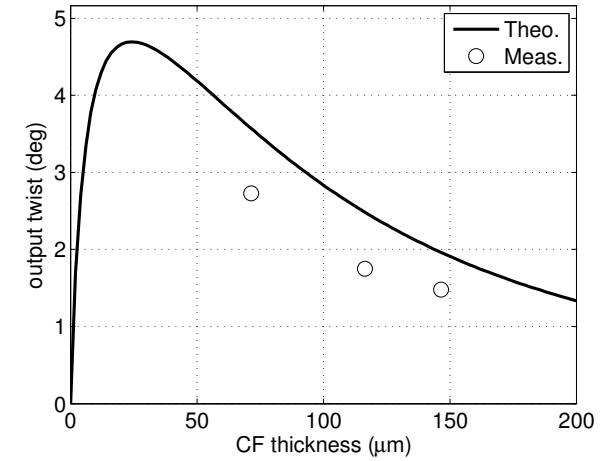

(a)

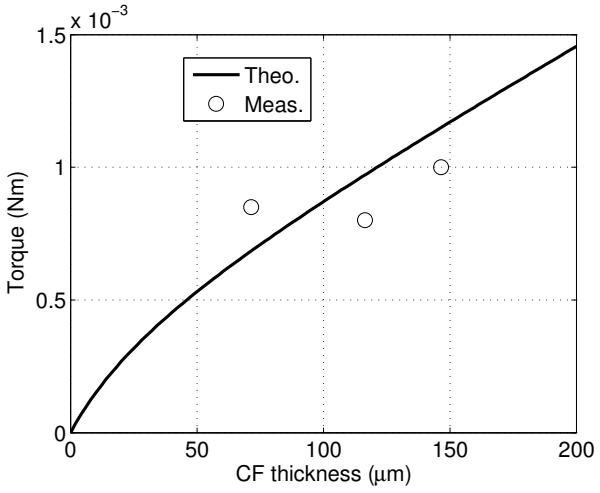

(b)

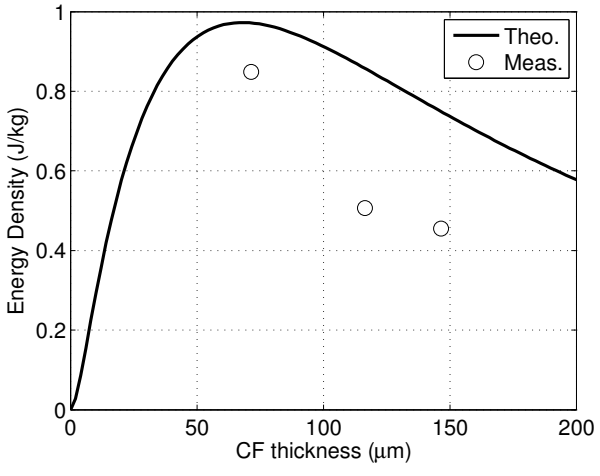

(c)

Fig. 6. (a) Actuator rotation vs. carbon fiber layer thickness, (b) blocked torque vs. thickness, and (c) energy density vs. thickness.

V. Conclusion

We have presented a theoretical model for a piezoelectric twisting actuator that utilizes an antisymmetric composite layup to exploit extension-twisting coupling. The model is used to predict actuator performance based on geometric parameters that can be varied experimentally, and these predictions are consistent with previous models. More importantly, empirical validation of the model shows that physical actuators do indeed have similar twist, torque and energy density magnitudes and follow trends predicted by the model for variation of geometric parameters. Actuator twist and torque are shown to scale linearly with length and width respectively, while both of these quantities are maximized at a composite layer orientation of $\pm 45^\circ$. Energy density is shown to be independent of length and width but is maximized for composite orientation of $\pm 45^\circ$ and composite layer thickness of 70μm, allowing optimization of energy density, which will be essential to high-performance, demanding applications.

References

[1] P. Luginbuhl, G. Racine, P. Lerch, B. Romanowicz, K. Brooks, N. De Rooij, P. Renaud, and N. Setter, "Piezoelectric cantilever beams actuated by PZT sol-gel thin film," *Sensors and Actuators A: Physical*, vol. 54, no. 1-3, pp. 530–535, 1996.

[2] C. Lee, T. Itoh, and T. Suga, "Self-excited piezoelectric PZT microcantilevers for dynamic SFM–with inherent sensing and actuating capabilities," *Sensors and Actuators A: Physical*, vol. 72, no. 2, pp. 179–188, 1999.

[3] R. Wood, E. Steltz, and R. Fearing, "Optimal energy density piezoelectric bending actuators," *Sensors and Actuators A: Physical*, vol. A 119, pp. 476–488, 2005.

[4] A. Dogan, Q. Xu, K. Onitsuka, S. Yoshikawa, K. Uchino, and R. Newnham, "High displacement ceramic metal composite actuators (moonies)," *Ferroelectrics*, vol. 156, no. 1, pp. 1–6, 1994.

[5] H. Van Lintel, F. Van de Pol, and S. Bouwstra, "A piezoelectric micropump based on micromachining of silicon," *Sensors and Actuators*, vol. 15, no. 2, pp. 153–167, 1988.

[6] S. Li and S. Chen, "Analytical analysis of a circular PZT actuator for valveless micropumps," *Sensors and Actuators A*, vol. 104, no. 2, pp. 151–161, 2003.

[7] A. Bernhard and I. Chopra, "Hover test of mach-scale active twist rotor using piezo-bending-torsion actuators," *Journal of aircraft*, vol. 39, no. 4, pp. 678–688, 2002.

[8] P. Chen and I. Chopra, "Hover testing of smart rotor with induced-strain actuation of blade twist," *AIAA journal*, vol. 35, no. 1, pp. 6–16, 1997.

[9] M.-L. Zhu, S.-W. Lee, H.-L. Li, T.-Y. Zhang, and P. Tong, "Modeling of torsional vibration induced by extension-twisting coupling of anisotropic composite laminates with piezoelectric actuators," *Smart Materials and Structures*, vol. 11, pp. 55–62, 2002.

[10] R. Wood, S. Avadhanula, R. Sahai, E. Steltz, and R. Fearing, "Microrobot Design Using Fiber Reinforced Composites," *Journal of Mechanical Design*, vol. 130, pp. 52 304–52 315, 2008.

[11] R. Jones, *Mechanics of composite materials*. CRC, 1999.

[12] R. Wood, "The first takeoff of a biologically inspired at-scale robotic insect," in *IEEE Transactions on Robotics*, vol. 24, no. 2, 2008, pp. 341–347.

[13] N. Perez-Arancibia, J. Whitney, and R. Wood, "Lift force control of a flapping-wing microrobot," in *Americal Controls Conference*, June 2011.

[14] "Piezo systems," 2010, www.piezo.com.